High-throughput computational design of Mo_3Al_2C-like noncentrosymmetric superconductors with multifold degenerate fermions

Jiexi Song,[1] Yanqing Qin,[1] Diwei Shi,[2,*] Xinyu Chen,[3] Wenqiang Li,[1] Yaocen Wang,[1,4] and Chongde Cao[1,4,†]

[1]*School of Physical Science and Technology, Northwestern Polytechnical University, Xian 710072, China*

[2]*School of Naval Architecture and Maritime, Zhejiang Ocean University, Zhoushan 316022, China*

[3]*School of Chemistry and Chemical Engineering, Nanjing University of Science and Technology, 200 Xiao Ling Wei Street, Nanjing 210094, China*

[4]*Research and Development Institute of Northwestern Polytechnical University in Shenzhen, Shenzhen 518057, China*

(Received 27 September 2023; accepted 2 January 2024; published 18 January 2024)

Nonsymmorphic chiral superconductors, like Mo_3Al_2C, are promising candidates to explore parity mixing and multifold degenerate fermions. However, only Mo_3Al_2C and W_3Al_2C in the Mo_3Al_2C family have been identified up to now. We carry out a high-throughput materials screening procedure on Mo_3Al_2C-like crystals based on first principles calculations. We report 21 crystals in this family based on systematic stability evaluations and perform electron-phonon coupling strength calculations for all of them. Additionally, the band structures of these compounds indicate that almost all of these compounds can hold multiple fermions near the Fermi level. This study may contribute to the discovery of more novel NCSs with multiple degenerate fermions.

DOI: 10.1103/PhysRevB.109.035144

I. INTRODUCTION

Recently, there has been an increasing interest in superconductors without inversion centers, called noncentrosymmetric superconductors (NCSs) [1–14]. An intriguing phenomenon arises in NCSs is the antisymmetric spin-orbit coupling (ASOC) effect, which makes the $(s+p)$-wave pairing below the superconducting transition temperature (T_c) possible [15]. This suggests that NCSs can hold the Majorana modes which can be manipulated to construct topological quantum computations [16,17]. Moreover, NCSs can exhibit distinctive characteristics that surpass conventional Bardeen-Cooper-Schrieffer (BCS) limits [18], including unconventional nodal gapless pairing [9], Ising superconductivity [19], and spontaneous time-reversal symmetry (TRS) breaking [9,20,21].

The research of NCSs was initiated following the discovery of unusual line nodes in the heavy fermion superconductor $CePt_3Si$ [1–3]. Several other compounds, such as $PbTaSe_2$ [22–26], $K_2Cr_3As_3$ [27], $LaNiC_2$ [4,20], Li_2Pt_3B [28–35], and Mo_3Al_2C [36–39], also display attractive superconducting and electronic properties. In recent years, significant attention has been paid to Mo_3Al_2C, which possesses a β-Mn-type structure with space group (SG) $P4_132$, having a relatively high $T_c = 9\,\mathrm{K}$ [39]. In this system, some observations suggest strong indications of the superconducting behavior deviating from the standard BCS model [39], while other techniques diagnose Mo_3Al_2C as nodeless electron pairing [40]. More recently, an isostructural compound of Mo_3Al_2C, that is, W_3Al_2C ($T_c = 7.6\,\mathrm{K}$), has been successfully synthesized, and a zero-field and transverse-field muon spin relaxation/rotation (μSR) measurement indicates the unconventional nature of superconductivity from the $T_c/\lambda_{\mathrm{eff}}^{-2}$ ratio [41,42].

More intriguingly, crystals with a SG number of 213 were proposed as excellent candidates for exploring exotic multiple degeneracy, i.e., sixfold degenerate fermions in the presence of TRS [43]. Although NCSs with Mo_3Al_2C structure contains a wealth of physical images, most of the exploratory work has been on Mo_3Al_2C and W_3Al_2C. In this work, a high-throughput screening based on first principles calculations has been carried out on NCSs with Mo_3Al_2C structure to obtain candidate materials with good stability for experimental synthesis. In addition, the electronic and superconducting properties have been calculated.

II. METHODOLOGY

The major calculations were carried out by using the Vienna *ab initio* simulation package (VASP) based on density function theory (DFT), and the projector augmented wave (PAW) method was utilized [44,45]. Besides, the Perdew-Burke-Ernzerhof (PBE) scheme within the framework of the generalized gradient approximation (GGA) for the exchange-correlation potential was utilized [46]. In order to reduce numerical errors, the pseudopotential types and the plane-wave basis energy cutoff (520 eV) were the same as that in the Materials Project (MP) [47] database. The force criterion was set to 0.001 eV/Å. Moreover, the Brillouin zone was sampled with a Γ-centered $5 \times 5 \times 5$ k-point mesh in relaxation and a $9 \times 9 \times 9$ k-point mesh in self-consistent calculation. In total, 2000 k points were utilized in band calculations. In phonon calculations, $2 \times 2 \times 2$ supercells were performed with the PHONOPY package and the density functional perturbation (DFPT) theory [48,49]. The maximally localized Wannier

*shidiwei@zjou.edu.cn
†caocd@nwpu.edu.cn

functions (MLWFs) were constructed with WANNIER90 [50] package and the Mo d orbital was utilized for the initial projection. In addition, the surface states were calculated with the WANNIERTOOLS [51] package. In addition, the VASPKIT [52] and PYPROCAR [53] codes were also used in data processing and figure plotting.

The electron-phonon coupling (EPC) strength calculations were carried out with the QUANTUM ESPRESSO (QE) package [54,55]. All structures were reoptimized using QE before electron-phonon calculations. The superconducting transition temperatures (T_c) were calculated from the Allen-Dynes equation [56,57].

$$T_c = \omega_{\log}\frac{f_1 f_2}{1.2}\exp\left[\frac{-1.04(1+\lambda)}{\lambda-\mu^*(1+0.62\lambda)}\right], \quad (1)$$

$$f_1 f_2 = \left[1+\left(\frac{\lambda}{2.46(1+3.8\mu^*)}\right)^{\frac{3}{2}}\right]^{\frac{1}{3}} \times \left[1-\frac{\left(1-\frac{\omega_2}{\omega_{\log}}\right)\lambda^2}{3.312(1+6.3\mu^*)^2+\lambda^2}\right], \quad (2)$$

where $\omega_{\log}$ stands for the logarithmic average frequency and ω_2 is the mean-square frequency. μ^* was set to 0.1 and the EPC constant (λ) can be defined as

$$\lambda = \sum_{qv}\lambda_{qv} = \int\frac{2\alpha^2 F(\omega)}{\omega}d\omega. \quad (3)$$

In QE calculations, the optimized norm-conserving Vanderbilt (ONCV) pseudopotentials were utilized [58]. The plane-wave basis energy cutoff was set to 60 Ry, the k-point mesh was set to $12\times12\times12$, and the q-point mesh was set to $4\times4\times4$.

III. RESULTS AND DISCUSSIONS

As can be found in Fig. 1(a), the Mo_3Al_2C-like compounds were labeled as M_3T_2X. The screening was started from element combinations based on M_3T_2X structure. Taking the element combinations of some already synthesized 3:2:1 compounds into account [41,59,60], in this work, M-site atoms were replaced with transition metals, Ti, Zr, Hf, V, Nb, Ta, Cr, Mo, W, Mn, Tc, Re, Fe, Ru, Os, Co, Rh, Ir, Ni, Pd, and Pt. T-site atoms were substituted with Cu, Ag, Au, Zn, Cd, Al, Ga, In, and Tl. X-site atoms were replaced with B, C, N, Si, P, Ge, and As, and 1323 phases in total were constructed and then were well relaxed by DFT calculations with switching symmetry on (ISYM = 2) and considering spin polarization (ISPIN = 2).

We then utilized the convex hull formation energy map to establish connections between phases that possess the lowest formation energy position at different compositions [61]. Generally, phases on the convex hull line (the energy above hull, i.e., $E_{\text{hull}} = 0$) are considered as thermodynamically stable. In addition, phases positioned above the convex hull ($E_{\text{hull}} > 0$) can be classified as thermodynamically metastable or unstable. A commonly used criterion for material synthesis is an E_{hull} value of 100 or 200 meV/atom; an E_{hull} below 50 meV/atom indicates a high success rate of synthesis [62–64]. We took the possible numerical errors in formation energy calculations or competing phases listed in the MP database into account. Then a medium threshold of 100 meV/atom was employed to screen out proper candidates with good thermodynamic stability that may be experimentally synthesized.

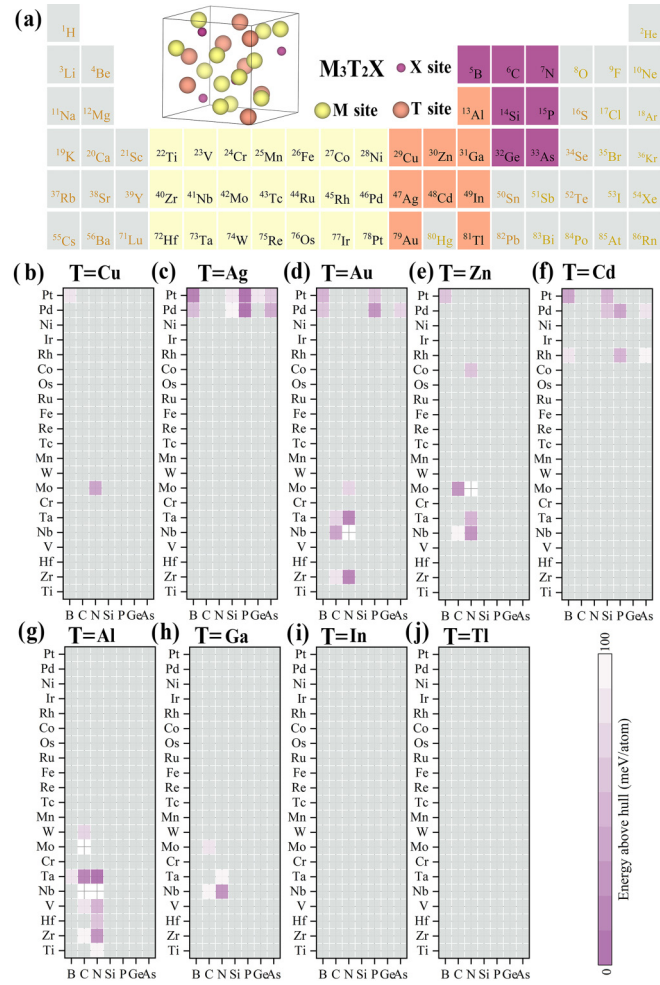

FIG. 1. (a) Crystal configuration of Mo_3Al_2C-like phases and the corresponding atomic site. (b)–(j) The results on hull energy calculation for each system with different T-site atoms. The gray rectangles indicate the hull energies are over 100 meV/atom.

Based on our DFT calculations, the PHASEDIAGRAM module [65] from PYMATGEN [66] was then used to calculate the E_{hull} for each constructed compound in this work combined with the MP database. The map of E_{hull} for each system with different T-site atoms from first-principles calculations and the MP database are shown in Figs. 1(b)–1(j). The gray rectangles indicate that the E_{hull} of related phases were more than 100 meV/atom. At first glance, we can find that a series of combinations satisfies the E_{hull} criterion where T-site atoms were substituted with Cu, Ag, Au, Zn, Cd, Al, and Ga. In addition, in the M_3In_2X and M_3Tl_2X systems, no phases show good thermodynamic stability. In this procedure, 55 phases were screened out.

The phonon spectrum can be utilized to check the dynamic stability of a specific solid crystal and a crystal can be verified as dynamically stable if its phonon dispersion displays without imaginary frequency modes. The calculated

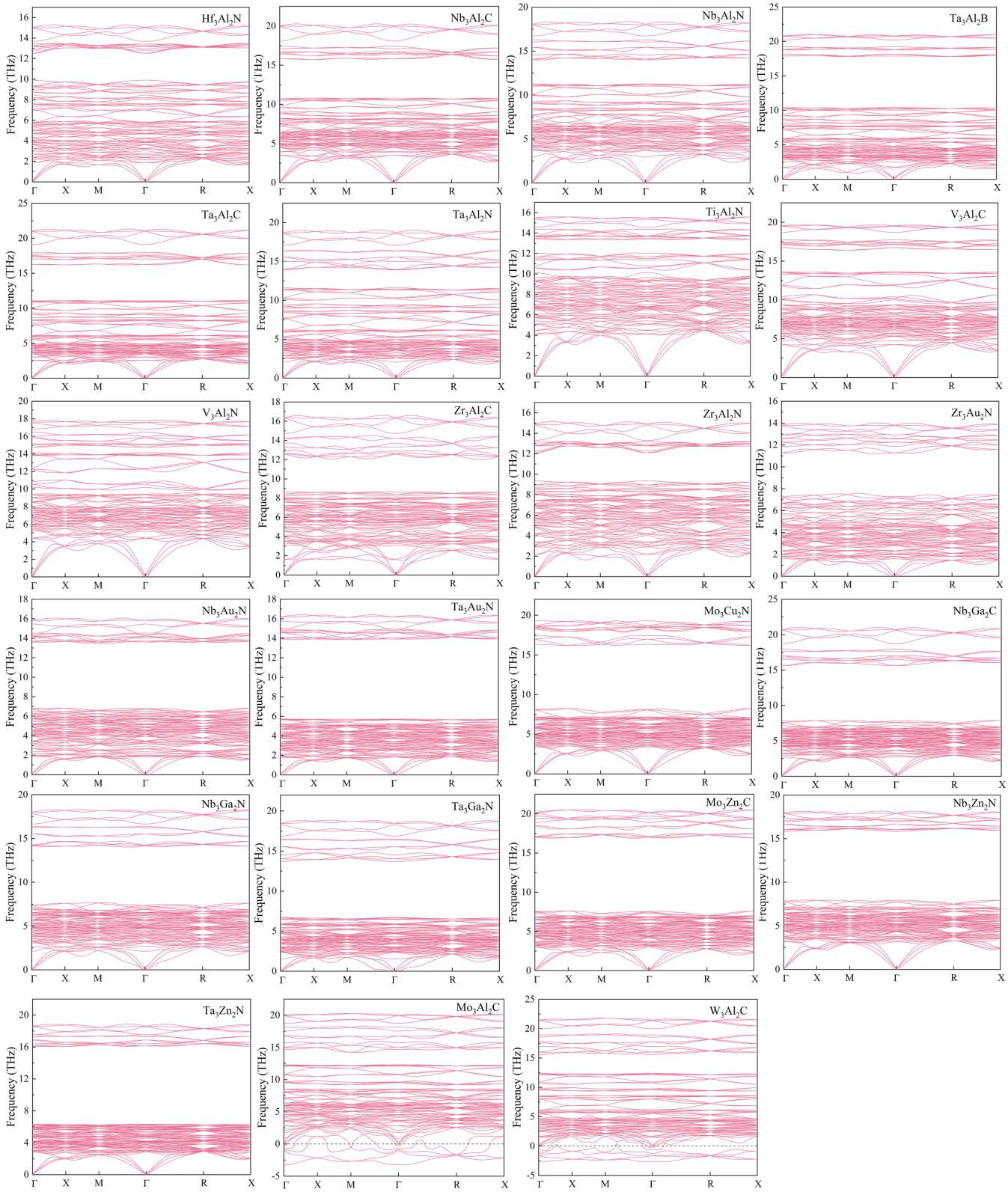

FIG. 2. Calculated phonon dispersions of Mo_3Al_2C, W_3Al_2C, and the other 21 Mo_3Al_2C-like compounds. The results show that except for Mo_3Al_2C and W_3Al_2C, the other 21 compounds are dynamically stable.

phonon spectra of these 55 compounds were displayed in Fig. 2 and Figs. S2–S5 in the Supplemental Material [67]. As we mentioned above, the parent structures Mo_3Al_2C and W_3Al_2C were retrieved from experimental x-ray diffraction data [39,42]. Intriguingly, we can find from Fig. 2 that Mo_3Al_2C and W_3Al_2C were dynamically unstable because large imaginary frequency modes occur, which indicated that intrinsic vacancies must appear to stabilize the crystal

TABLE I. The calculated lattice parameters, independent elastic constants C_{ij}, Vickers hardness, and averaged band splitting energies at Fermi level E_{ASOC} of the 23 Mo_3Al_2C-like compounds with good thermodynamic and dynamic stabilities.

Phase	a (Å)	C_{11} (GPa)	C_{12} (GPa)	C_{44} (GPa)	Vickers hardness (GPa)	E_{ASOC} (meV)
Hf_3Al_2N	7.311	270.508	92.307	90.072	12.210	43.2
Nb_3Al_2C	7.129	321.232	123.522	124.802	14.693	27.1
Nb_3Al_2N	7.077	330.339	128.945	121.907	13.955	24.0
Ta_3Al_2B	7.179	308.610	125.130	123.257	13.975	91.2
Ta_3Al_2C	7.090	347.828	136.119	135.982	15.389	52.6
Ta_3Al_2N	7.039	353.990	142.363	132.100	14.406	71.4
Ti_3Al_2N	6.923	290.382	86.344	106.256	15.886	2.3
V_3Al_2C	6.674	329.323	116.726	132.019	16.681	9.0
V_3Al_2N	6.627	342.584	120.538	128.991	16.108	10.6
Zr_3Al_2C	7.477	229.582	82.920	80.629	10.977	10.1
Zr_3Al_2N	7.395	251.231	84.421	85.700	12.056	8.6
Zr_3Au_2N	7.417	222.937	132.484	86.539	6.533	53.3
Nb_3Au_2N	7.170	326.233	156.737	97.770	8.749	57.8
Ta_3Au_2N	7.137	351.895	173.563	103.072	8.707	61.2
Mo_3Cu_2N	6.708	385.133	178.043	139.962	12.759	32.7
Nb_3Ga_2C	7.107	308.072	128.648	112.266	12.236	25.4
Nb_3Ga_2N	7.059	312.650	135.770	105.441	10.884	25.7
Ta_3Ga_2N	7.028	324.263	154.135	111.559	10.282	65.7
Mo_3Zn_2C	6.845	344.194	154.726	129.116	12.607	49.5
Nb_3Zn_2N	7.035	322.448	121.071	118.288	14.141	18.0
Ta_3Zn_2N	6.996	357.177	133.982	128.932	14.948	72.6
Mo_3Al_2C	6.875	297.914	189.648	105.614	6.406	28.9
W_3Al_2C	6.889	312.361	219.862	135.712	6.692	90.1

lattice. We then calculated the phonon spectra of Mo_3Al_2C and W_3Al_2C with vacancies and the results confirmed that these vacancy structures could become dynamically stable, which was in accordance with previous reports [38,41], as shown in Fig. S1 in the Supplemental Material [67].

Additionally, the mechanical stability of those compounds was also evaluated. In the case of compounds belonging to the cubic crystal class, three independent elastic constants (C_{ij}) are necessary for the assessment. To be considered mechanically stable, a cubic crystal must meet the following conditions: $C_{11} > C_{12}$, $C_{11} + 2C_{12} > 0$ and $C_{44} > 0$ [68]. The calculated elastic constants can be found in Table I. Obviously, all of the 23 compounds were predicted to be mechanically stable. Moreover, we find that V_3Al_2N and V_3Al_2C have relatively larger Vickers hardness [69] (>16 GPa) than other compounds. Conversely, the Vickers hardness of Mo_3Al_2C and W_3Al_2C was around 6.5 GPa.

After implementing such a comprehensive stability filtering frame, a total of 23 compounds (including previously reported Mo_3Al_2C and W_3Al_2C) emerged as promising candidate materials. Subsequently, we conducted calculations to determine the electronic properties of these compounds. The calculated energy bands with and without considering the spin-orbital coupling (SOC) effect of these compounds were displayed in Fig. 3 and Fig. S6 in the Supplemental Material [67]. The Brillouin zone and selected K path can be found in Fig. 4(a).

In general, the strength of ASOC was found to play a significant role in determining the gap symmetry of NCSs due to the fact that many unconventional NCSs like $CePt_3Si$, CaPtAs, $ThCoC_2$, and Li_2Pt_3B have a large band splitting at the Fermi energy (E_f) [15,70,71], and the corresponding splitting energy of a NCS at E_f from a DFT band calculation with SOC can be denoted as E_{ASOC} [15]. For example, the effect of ASOC on gap symmetry has been directly observed in the well-known system $Li_2(Pd, Pt)_3B$ compound [28,30,31]. In this system, the parent phase Li_2Pd_3B is demonstrated as a conventional BCS superconductor while Li_2Pd_3B can transform from s-wave to $(s + p)$ wave pairing with the introduction of Pt substitution to $Li_2(Pd_{1-x}Pt_x)_3B$, i.e., with the increasing ASOC strength from the presence of heavier Pt atoms than Pd. The similarity in the case of $Li_2(Pd, Pt)_3B$ and $(Mo, W)_3Al_2C$ both emphasize the pronounced effect of ASOC on superconducting pairing.

More intuitively, we listed some reported values of E_{ASOC} for some famous unconventional NCSs, which either possess nodal-line superconductivity or exhibit a spin-triplet dominated pairing state. Specifically, E_{ASOC} values of 150, 200, 200, 50–100, and 40 meV were reported for $ThCoC_2$ [71], $CePt_3Si$ and Li_2Pt_3B [15], CaPtAs [70], and $LaNiC_2$ [4], respectively. In contrast, BiPd [72,73] and Li_2Pd_3B [15], two conventional superconductors, were found to exhibit E_{ASOC} values of 50 and 30 meV, respectively. These previous reports reveal that a large E_{ASOC} seems to be a prerequisite, though not sufficient, for the emergence of notable mixed parity pairing.

More intriguingly, Rashba-like SOC is recognized to arise as the mirror symmetry breaking [15]. In NCSs, the Rashba-like SOC typically exerts a direct influence on the spin susceptibility structure in the normal state [74], and a pronounced Rashba effect is advantageous for electrons to counteract the suppressive impact of the Zeeman field on superconductivity [74,75]. Thus it is reasonable to anticipate that a stronger ASOC or a larger E_{ASOC} in NCSs without mirror symmetry such as the Mo_3Al_2C-like compounds could

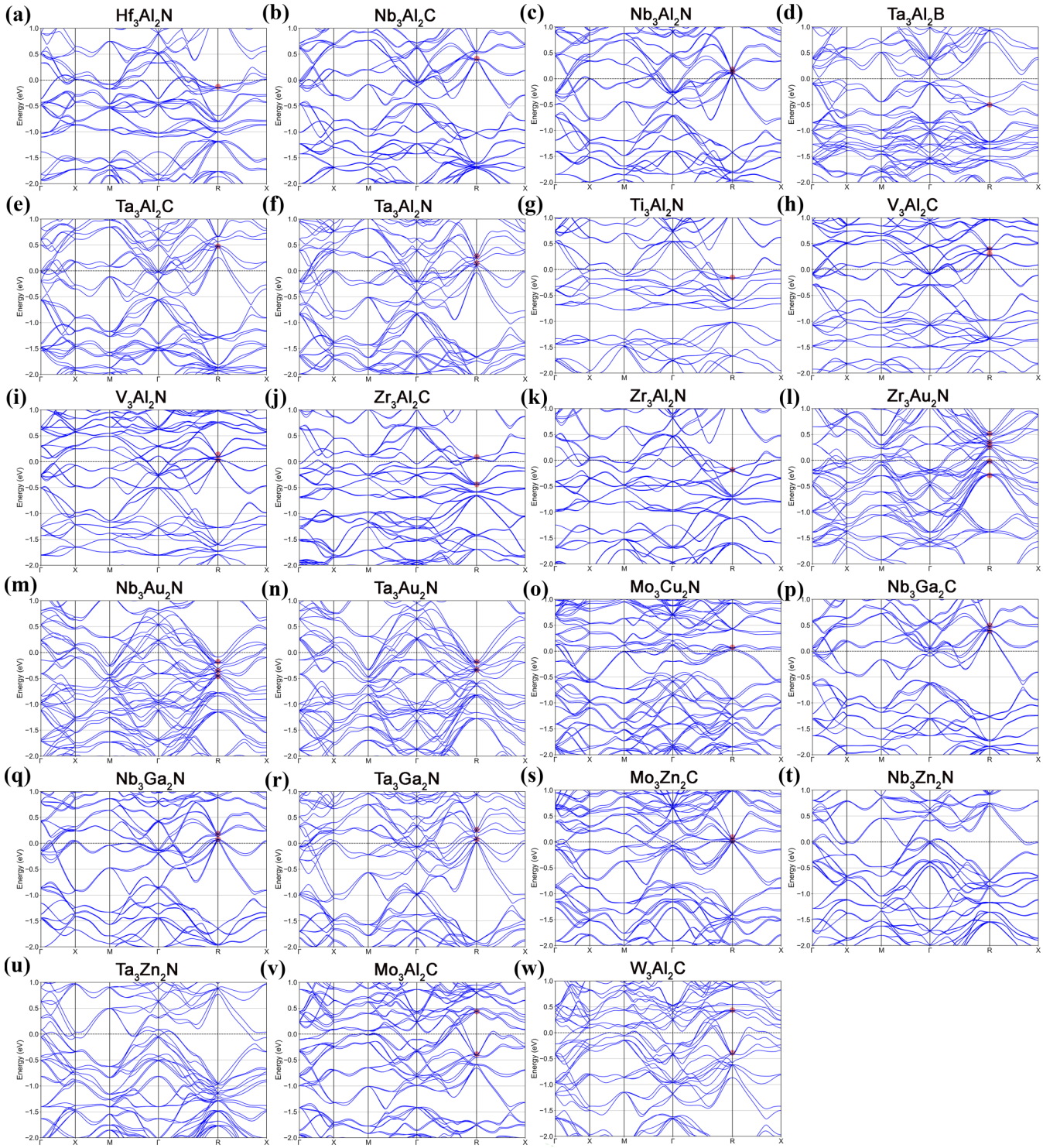

FIG. 3. (a)–(w) The energy bands of 23 Mo_3Al_2C-like phases with considering SOC. The red circles denote the sixfold degeneracy around the Fermi level.

increase the likelihood of unconventional superconductivity. For example, we calculated the spin projected Fermi surfaces around the Γ point of Mo_3Zn_2C with considering SOC, and the results displayed the Rashba-like spin texture, as shown in Fig. S8 in the Supplemental Material [67].

In order to determine the effective points surrounding E_f for measuring E_{ASOC}, 2000 k points in total were utilized to calculate the energy bands; the energy eigenvalues were then computed. An additional constraint was implemented in this procedure, whereby only k points with one eigenvalue below E_f and the other above E_f were chosen for calculating the averaged SOC splitting. The predicted E_{ASOC}'s for these compounds are listed in Table I. We find that five compounds, Ti_3Al_2N, V_3Al_2C, V_3Al_2N, Zr_3Al_2C, and Zr_3Al_2N, had very

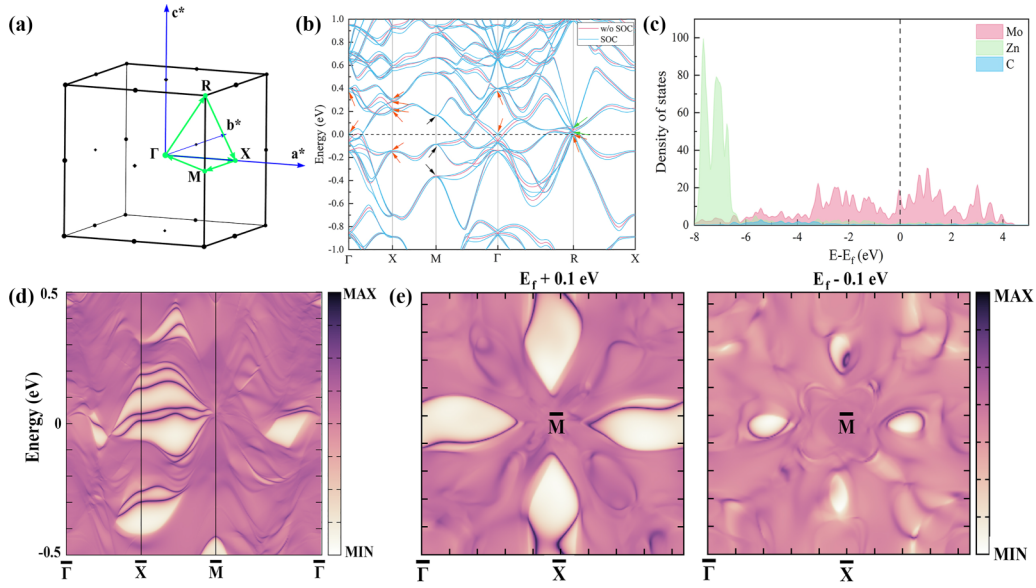

FIG. 4. (a) The Brillouin zone and selected K path of Mo_3Al_2C-like compounds. (b) Energy bands of Mo_3Zn_2C with and without SOC. (c) The projected density of states of Mo_3Zn_2C. (d) The surface band spectrum projected on the (001) surface and (e) the surface band spectra at a specific energy level of Mo_3Zn_2C. The orange, black, and green arrows point out the Kramers-Weyl, dKramers-Weyl, and sixfold degeneracies around the E_f, respectively.

small E_{ASOC}, only around 10 meV, while most of the other compounds had a medium E_{ASOC} value around 50 meV. This may indicate that parity mixing should be small in Mo_3Al_2C-like compounds.

Recently, there has been a proposal suggesting that the presence of TRS and specific crystal symmetries in some solids can safeguard the existence of exotic fermions with degeneracies of three-, six- or eightfold [43]. This is particularly fascinating because such fermions do not have any counterparts in the realm of high-energy physics, primarily due to the constraints imposed by Poincaré symmetry [43,76,77]. The multifold fermions can originate from specific operations at particular high-symmetry points. In the case of Mo_3Al_2C-like compounds, the R $(\pi/a, \pi/a, \pi/a)$ point can hold sixfold fermions from the following rotation operations: $\{C_{3,111}^{-1}|000\}$, $\{C_{2x}|\frac{1}{2}\frac{1}{2}0\}$, $\{C_{2y}|\frac{1}{2}\frac{1}{2}0\}$, and $\{C_{2,1\bar{1}0}|\frac{3}{4}\frac{3}{4}\frac{3}{4}\}$ [43]. As can be found in Fig. 3, the sixfold fermions of these compounds around the E_f (± 0.5 eV) are marked with red circles. The fact that almost all Mo_3Al_2C-like compounds have sixfold degeneracies around the E_f suggests that members of this family are promising candidates to detect sixfold fermions.

More intriguingly, as one of the 41 nonsymmorphic chiral SGs, Mo_3Al_2C-like compounds with SG 213 were proposed as promising candidates to explore Kramers-Weyl fermions at high-symmetry points. Generally, Kramers-Weyl fermions are distinct from other types of fermions as they do not arise from a band inversion nor rely on specific crystal symmetries [78,79]. Their existence as chiral fermions is ensured solely by the influence of TRS on the irreducible representations of the chiral point groups. Kramers-Weyl fermions, in contrast to other chiral fermions, can only be annihilated through pairwise interactions, for example, which may be achievable by subjecting them to a very strong magnetic field. Consequently, Kramers-Weyl fermions exhibit heightened resilience against external disturbances and thus become more robust compared to other chiral fermions [78].

We take Mo_3Zn_2C as an example; the corresponding Kramers-Weyl, double Kramers-Weyl (doubled by nonsymmorphic symmetries), and sixfold degeneracies around the E_f are marked with different arrows, as shown in Fig. 4(b). We can see from Fig. 4(b) that obvious band splitting occurs when considering SOC, and the Kramers-Weyl band crossing point (marked in orange arrows) appears in pairs. To further investigate the surface states of Mo_3Zn_2C, we then constructed the MLWFs. As can be found in Fig. 4(c), the projected density of states (PDOS) indicates that the contribution of Mo atoms dominates around the E_f. Consequently, we choose Mo d orbitals as initial projectors. The calculated energy bands from GGA+PBE and MLWFs of Mo_3Zn_2C with considering SOC can be found in Fig. S7 [67]. We then calculated the surface band structures projected on the (001) surface of Mo_3Zn_2C based on the constructed MLWFs. As can be found in Fig. 4(d), clear surface states can be detected at E_f. Moreover, we then calculated the surface states of Mo_3Zn_2C for a different energy scheme. As shown in Fig. 4(e), nontrivial surface states were found to be almost buried in bulk states. This may indicate that the surface states of Mo_3Zn_2C were only detectable around a narrow energy range. All the same, Mo_3Zn_2C still becomes a promising candidate material for having Kramers-Weyl, double Kramers-Weyl, and sixfold band degeneracies around E_f simultaneously, which may be rare among numerous topological material families.

We then focus on the superconducting properties of these compounds. As we mentioned above, the pure lattice of Mo_3Al_2C and W_3Al_2C were dynamically unstable, which indicated that the intrinsic vacancies must appear. However, the EPC calculations on defective structures with massive vibrational modes were extremely expensive. Thus we performed electron-phonon coupling strength calculations on

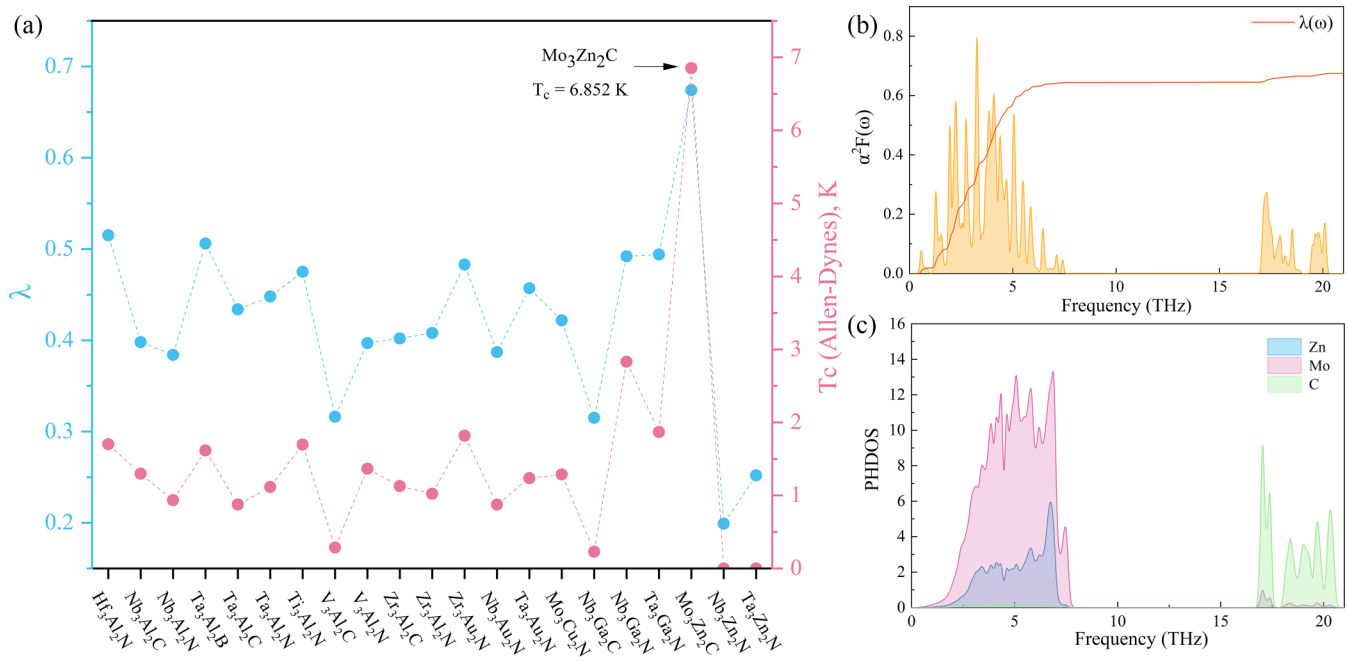

FIG. 5. (a) Superconducting properties of the 21 Mo_3Al_2C-like compounds that were predicted in this work. (b) Eliashberg spectrum functions $\alpha^2F(\omega)$ and the integral EPC parameters $\lambda(\omega)$ of Mo_3Zn_2C. (c) The projected phonon density of states of Mo_3Zn_2C.

21 Mo_3Al_2C-like compounds that were dynamically stable and predicted in this work. As can be found in Fig. 5(a), Nb_3Zn_2N and Ta_3Zn_2N were calculated to be nonsuperconducting phases and the T_c's of V_3Al_2C and Nb_3Ga_2C were lower than 0.5 K. Moreover, we can find that Mo_3Zn_2C was predicted to have the highest λ of 0.674 and T_c of 6.852 K among these compounds, and the T_c's of the rest of the compounds were predicted around 2 K, displaying weak to medium coupling. The Eliashberg spectrum functions $\alpha^2F(\omega)$, integral EPC parameters $\lambda(\omega)$, and the projected phonon density of states (PHDOS) of Mo_3Zn_2C were shown in Figs. 5(b) and 5(c). From PHDOS, we find that the phonon dispersions of Mo_3Zn_2C consisted of two parts: the low-frequency region was mainly contributed to the vibrations of Mo and Zn atoms and the high-frequency region mainly had origins in the vibrations of carbon atoms. The results on EPC strength in Mo_3Zn_2C indicated that superconductivity of Mo_3Zn_2C was mainly contributed to the metal atom region at low frequency. The detailed superconducting parameters calculated in this work are listed in Table S1 [67].

Note that the T_c calculated from the Allen-Dynes equation can only represent the conventional superconducting transition. Consequently, we also calculated the T_c of these compounds based on machine learning models, the training set of which contained a series of unconventional superconductors like iron-based superconductors and cuprate superconductors like $YBa_2Cu_3O_7$ [80]. The predicted T_c from machine learning (ML) models are listed in Table S2 [67]. Both models indicated Mo_3Al_2C and W_3Al_2C were superconductors and the predicted T_c's of Mo_3Al_2C (3.42 K) and W_3 Al_2C (4.62 K) were underestimated and lower than experimental data. In addition, we can find from Table S2 [67] that 15 compounds in total predicted in this work were found to be superconducting from both ML models. Compared with the T_c results calculated from the Allen-Dynes equation, we can infer that these compounds, Nb_3Al_2C, Ta_3Al_2B, Ta_3Al_2C, V_3Al_2N, Zr_3Al_2N, Zr_3Au_2N, Nb_3Au_2N, Ta_3Au_2N, Mo_3Cu_2N, Nb_3Ga_2N, Ta_3Ga_2N, and particularly Mo_3Zn_2C which has the highest λ, were promising candidates to investigate superconducting transitions in the Mo_3Al_2C family.

IV. CONCLUSIONS

In summary, we employed high-throughput calculations through density functional theory on Mo_3Al_2C-like noncentrosymmetric superconductors. Twenty-three compounds with good thermodynamic, dynamic, and mechanical stabilities were identified as promising candidates for experimental analysis among the 1323 crystals calculated in this work. Additionally, we calculated the band structures with SOC of these compounds and the results indicated that these compounds can hold multiple fermions including Kramers-Weyl, double Kramers-Weyl, and sixfold fermions. Moreover, we have performed electron-phonon interaction calculations on compounds predicted in this work, and Mo_3Zn_2C was predicted to have a relatively high T_c of 6.852 K. Besides the T_c results calculated from the Allen-Dynes equation, we also calculated the T_c of these compounds based on machine learning models. The results show the Mo_3Al_2C-like family is a promising platform to explore superconductivity and topological excitation. We hope that our results may contribute to the discovery of more novel superconductors without inversion centers and topological quantum materials with multiple degeneracies.

The data that support the findings of this study are available from the corresponding author upon reasonable request.

ACKNOWLEDGMENTS

This work is supported by the National Natural Science Foundation of China (Grants No. 51971180, No. 52271037, and No. 51971179), the Key Research Program of Chinese Academy of Sciences (Grant No. ZDBS-ZRKJZ-TLC021), the Scientific Research Foundation for the Introduction of Talent of Zhejiang Ocean University (Grant No. 11185091722), Shaanxi Provincial Science and Technology Program, China (Grant No. 2023-JC-ZD-23), and Shenzhen Fundamental Research Program, China (Grant No. JCYJ20210324122203010). Part of the calculations were performed in the High Performance Computation Center of Northwestern Polytechnical University. The authors are very grateful to Mr. Zhenyu Liu for providing high-performance computers.

Author contributions are as follows: J.S.:c, calculation, data analysis, preparation of paper; Y.Q.: data acquisition, visualization; D.S.: calculation, software; X.C.: data analysis, discussion; W.L.: discussion; Y.W.: discussion; C.C.: paper editing and review, supervision, funding acquisition.

There are no conflicts of interest to declare.

[1] K. V. Samokhin, E. S. Zijlstra, and S. K. Bose, $CePt_3Si$: An unconventional superconductor without inversion center, Phys. Rev. B **69**, 094514 (2004).

[2] I. Bonalde, W. Brämer-Escamilla, and E. Bauer, Evidence for line nodes in the superconducting energy gap of noncentrosymmetric $CePt_3Si$ from magnetic penetration depth measurements, Phys. Rev. Lett. **94**, 207002 (2005).

[3] H. Mukuda, S. Nishide, A. Harada, K. Iwasaki, M. Yogi, M. Yashima, Y. Kitaoka, M. Tsujino, T. Takeuchi, R. Settai, Y. Ōnuki, E. Bauer, K. M. Itoh, and E. E. Haller, Multiband superconductivity in heavy fermion compound $CePt_3Si$ without inversion symmetry: An NMR study on a high-quality single crystal, J. Phys. Soc. Jpn. **78**, 014705 (2009).

[4] A. Subedi and D. J. Singh, Electron-phonon superconductivity in noncentrosymmetric $LaNiC_2$: First-principles calculations, Phys. Rev. B **80**, 092506 (2009).

[5] B. Li, C. Q. Xu, W. Zhou, W. H. Jiao, R. Sankar, F. M. Zhang, H. H. Hou, X. F. Jiang, B. Qian, B. Chen, A. F. Bangura, and X. Xu, Evidence of *s*-wave superconductivity in the noncentrosymmetric La_7Ir_3, Sci. Rep. **8**, 651 (2018).

[6] H. Y. Uzunok, H. M. Tütüncü, G. P. Srivastava, and A. Başoğlu, Theoretical investigation of superconductivity in the non-centrosymmetric $SrPtGe_3$ and $CaPtSi_3$ compounds, Philos. Mag. **99**, 198 (2018).

[7] A. Bhattacharyya, D. T. Adroja, K. Panda, S. Saha, T. Das, A. J. S. Machado, O. V. Cigarroa, T. W. Grant, Z. Fisk, A. D. Hillier, and P. Manfrinetti, Evidence of a nodal line in the superconducting gap symmetry of noncentrosymmetric $ThCoC_2$, Phys. Rev. Lett. **122**, 147001 (2019).

[8] A. Ptok, K. Domieracki, K. J. Kapcia, J. Łażewski, P. T. Jochym, M. Sternik, P. Piekarz, and D. Kaczorowski, Electronic and lattice properties of noncentrosymmetric superconductors Th*T*Si (T = Co, Ir, Ni, and Pt), Phys. Rev. B **100**, 165130 (2019).

[9] T. Shang, M. Smidman, A. Wang, L. J. Chang, C. Baines, M. K. Lee, Z. Y. Nie, G. M. Pang, W. Xie, W. B. Jiang, M. Shi, M. Medarde, T. Shiroka, and H. Q. Yuan, Simultaneous nodal superconductivity and time-reversal symmetry breaking in the noncentrosymmetric superconductor CaPtAs, Phys. Rev. Lett. **124**, 207001 (2020).

[10] H. Y. Uzunok, T. Zafer, H. M. Tütüncü, E. r. Karaca, S. Bağcı, and G. P. Srivastava, Probing physical properties and superconductivity of noncentrosymmetric superconductors LaPtGe and $LaPtGe_3$: A first-principles study, Comput. Mater. Sci. **185**, 109949 (2020).

[11] P. Zhang, H. Yuan, and C. Cao, Electron-phonon coupling and nontrivial band topology in noncentrosymmetric superconductors LaNiSi, LaPtSi, and LaPtGe, Phys. Rev. B **101**, 245145 (2020).

[12] A. Iyo, I. Hase, H. Fujihisa, Y. Gotoh, S. Ishida, H. Ninomiya, Y. Yoshida, H. Eisaki, H. T. Hirose, T. Terashima, and K. Kawashima, Antiperovskite superconductor $LaPd_3P$ with noncentrosymmetric cubic structure, Inorg. Chem. **60**, 18017 (2021).

[13] J. Song, D. Shi, Y. Qin, X. Chen, W. Li, P. Qin, R. Ren, Y. Wang, X. Bai, X. Yang, and C. Cao, First-principles study of topological surface states and pressure induced phase transitions in a novel noncentrosymmetric superconductor $PbTiSe_2$, Comput. Mater. Sci. **218**, 111982 (2023).

[14] J. Song, Y. Qin, Y. Wang, and C. Cao, Superconductivity and topologically nontrivial states in noncentrosymmetric $XVSe_2$ (X = Pb, Sn): A first-principles study, Phys. Chem. Chem. Phys. **24**, 1770 (2022).

[15] M. Smidman, M. B. Salamon, H. Q. Yuan, and D. F. Agterberg, Superconductivity and spin-orbit coupling in noncentrosymmetric materials: A review, Rep. Prog. Phys. **80**, 036501 (2017).

[16] T. Karzig, C. Knapp, R. M. Lutchyn, P. Bonderson, M. B. Hastings, C. Nayak, J. Alicea, K. Flensberg, S. Plugge, Y. Oreg, C. M. Marcus, and M. H. Freedman, Scalable designs for quasiparticle-poisoning-protected topological quantum computation with Majorana zero modes, Phys. Rev. B **95**, 235305 (2017).

[17] Y. Oreg and F. von Oppen, Majorana zero modes in networks of Cooper-pair boxes: Topologically ordered states and topological quantum computation, Annu. Rev. Condens. Matter Phys. **11**, 397 (2020).

[18] H. Suhl, B. T. Matthias, and L. R. Walker, Bardeen-Cooper-Schrieffer theory of superconductivity in the case of overlapping bands, Phys. Rev. Lett. **3**, 552 (1959).

[19] P. Samuely, P. Szabó, J. Kačmarčík, A. Meerschaut, L. Cario, A. G. M. Jansen, T. Cren, M. Kuzmiak, O. Šofranko, and T. Samuely, Extreme in-plane upper critical magnetic fields of heavily doped quasi-two-dimensional transition metal dichalcogenides, Phys. Rev. B **104**, 224507 (2021).

[20] A. D. Hillier, J. Quintanilla, and R. Cywinski, Evidence for time-reversal symmetry breaking in the noncentrosymmetric superconductor $LaNiC_2$, Phys. Rev. Lett. **102**, 117007 (2009).

[21] S. Ghosh, M. Smidman, T. Shang, J. F. Annett, A. D. Hillier, J. Quintanilla, and H. Yuan, Recent progress on superconductors with time-reversal symmetry breaking, J. Phys.: Condens. Matter **33**, 033001 (2020).

[22] G. Bian, T. R. Chang, R. Sankar, S. Y. Xu, H. Zheng, T. Neupert, C. K. Chiu, S. M. Huang, G. Chang, I. Belopolski, D. S. Sanchez, M. Neupane, N. Alidoust, C. Liu, B. Wang, C. C. Lee, H. T. Jeng, C. Zhang, Z. Yuan, S. Jia *et al.*, Topological nodal-line fermions in spin-orbit metal $PbTaSe_2$, Nat. Commun. **7**, 10556 (2016).

[23] T.-R. Chang, P.-J. Chen, G. Bian, S.-M. Huang, H. Zheng, T. Neupert, R. Sankar, S.-Y. Xu, I. Belopolski, G. Chang, B. Wang, F. Chou, A. Bansil, H.-T. Jeng, H. Lin, and M. Z. Hasan, Topological Dirac surface states and superconducting pairing correlations in $PbTaSe_2$, Phys. Rev. B **93**, 245130 (2016).

[24] S. Y. Guan, P. J. Chen, M. W. Chu, R. Sankar, F. Chou, H. T. Jeng, C. S. Chang, and T. M. Chuang, Superconducting topological surface states in the noncentrosymmetric bulk superconductor $PbTaSe_2$, Sci. Adv. **2**, e1600894 (2016).

[25] X. Xu, Z. Kang, T.-R. Chang, H. Lin, G. Bian, Z. Yuan, Z. Qu, J. Zhang, and S. Jia, Quantum oscillations in the noncentrosymmetric superconductor and topological nodal-line semimetal $PbTaSe_2$, Phys. Rev. B **99**, 104516 (2019).

[26] T. Le, Y. Sun, H.-K. Jin, L. Che, L. Yin, J. Li, G. Pang, C. Xu, L. Zhao, S. Kittaka, T. Sakakibara, K. Machida, R. Sankar, H. Yuan, G. Chen, X. Xu, S. Li, Y. Zhou, and X. Lu, Evidence for nematic superconductivity of topological surface states in $PbTaSe_2$, Sci. Bull. **65**, 1349 (2020).

[27] J. Yang, J. Luo, C. Yi, Y. Shi, Y. Zhou, and G.-q. Zheng, Spin-triplet superconductivity in $K_2Cr_3As_3$, Sci. Adv. **7**, eabl4432 (2021).

[28] S. K. Bose and E. S. Zijlstra, Electronic structure, electron–phonon coupling and superconductivity of isotypic noncentrosymmetric crystals Li_2Pd_3B and Li_2Pt_3B, Physica C (Amsterdam) **432**, 173 (2005).

[29] S. Chandra, S. M. Jaya, and M. C. Valsakumar, Electronic structure of Li_2Pd_3B and Li_2Pt_3B, Physica C (Amsterdam) **432**, 116 (2005).

[30] K. W. Lee and W. E. Pickett, Crystal symmetry, electron-phonon coupling, and superconducting tendencies in Li_2Pd_3B and Li_2Pt_3B, Phys. Rev. B **72**, 174505 (2005).

[31] H. Takeya, K. Hirata, K. Yamaura, K. Togano, M. El Massalami, R. Rapp, F. A. Chaves, and B. Ouladdiaf, Low-temperature specific-heat and neutron-diffraction studies on Li_2Pd_3B and Li_2Pt_3B superconductors, Phys. Rev. B **72**, 104506 (2005).

[32] H. Q. Yuan, D. F. Agterberg, N. Hayashi, P. Badica, D. Vandervelde, K. Togano, M. Sigrist, and M. B. Salamon, *S*-wave spin-triplet order in superconductors without inversion symmetry: Li_2Pd_3B and Li_2Pt_3B, Phys. Rev. Lett. **97**, 017006 (2006).

[33] A. Shimamura, Y. Furukawa, K. Kumagai, H. Takeya, and K. Hirata, NMR study of noncentrosymmetric superconductor Li_2Pt_3B, Physica C (Amsterdam) **460-462**, 663 (2007).

[34] C. F. Miclea, A. C. Mota, M. Sigrist, F. Steglich, T. A. Sayles, B. J. Taylor, C. A. McElroy, and M. B. Maple, Vortex avalanches in the noncentrosymmetric superconductor Li_2Pt_3B, Phys. Rev. B **80**, 132502 (2009).

[35] S. P. Mukherjee and T. Takimoto, Order parameter with line nodes and $s\pm$-wave symmetry for the noncentrosymmetric superconductor Li_2Pt_3B, Phys. Rev. B **86**, 134526 (2012).

[36] T. Koyama, Y. Ozaki, K. Ueda, T. Mito, T. Kohara, T. Waki, Y. Tabata, C. Michioka, K. Yoshimura, M. T. Suzuki, and H. Nakamura, Partial gap opening on the Fermi surface of the noncentrosymmetric superconductor Mo_3Al_2C, Phys. Rev. B **84**, 212501 (2011).

[37] T. Koyama, Y. Ozaki, K. Ueda, T. Mito, T. Kohara, T. Waki, Y. Tabata, and H. Nakamura, Phase transition in the normal state of the non-centrosymmetric superconductor Mo_3Al_2C, J. Phys.: Conf. Ser. **391**, 012097 (2012).

[38] D. Reith, C. Blaas-Schenner, and R. Podloucky, Density functional theory study of phase stability, vibrational, and electronic properties of Mo_3Al_2C, Phys. Rev. B **86**, 104105 (2012).

[39] E. Bauer, G. Rogl, X.-Q. Chen, R. T. Khan, H. Michor, G. Hilscher, E. Royanian, K. Kumagai, D. Z. Li, Y. Y. Li, R. Podloucky, and P. Rogl, Unconventional superconducting phase in the weakly correlated noncentrosymmetric Mo_3Al_2C compound, Phys. Rev. B **82**, 064511 (2010).

[40] E. Bauer, C. Sekine, U. Sai, P. Rogl, P. K. Biswas, and A. Amato, Absence of time-reversal symmetry breaking in the noncentrosymmetric superconductor Mo_3Al_2C, Phys. Rev. B **90**, 054522 (2014).

[41] T. Ying, Y. Muraba, S. Iimura, T. Yu, P. Cheng, T. Kamiya, Y. Lu, J. Li, Y. Qi, and H. Hosono, Anomalous charge state evolution and its control of superconductivity in M_3Al_2C (M = Mo, W), iScience **23**, 101196 (2020).

[42] R. Gupta, T. P. Ying, Y. P. Qi, H. Hosono, and R. Khasanov, Gap symmetry of the noncentrosymmetric superconductor W_3Al_2C, Phys. Rev. B **103**, 174511 (2021).

[43] B. Bradlyn, J. Cano, Z. Wang, M. G. Vergniory, C. Felser, R. J. Cava, and B. A. Bernevig, Beyond Dirac and Weyl fermions: Unconventional quasiparticles in conventional crystals, Science **353**, aaf5037 (2016).

[44] G. Kresse and J. Furthmüller, Efficiency of *ab-initio* total energy calculations for metals and semiconductors using a plane-wave basis set, Comput. Mater. Sci. **6**, 15 (1996).

[45] G. Kresse and J. Furthmüller, Efficient iterative schemes for *ab initio* total-energy calculations using a plane-wave basis set, Phys. Rev. B **54**, 11169 (1996).

[46] J. P. Perdew, K. Burke, and M. Ernzerhof, Generalized gradient approximation made simple, Phys. Rev. Lett. **77**, 3865 (1996).

[47] A. Jain, S. P. Ong, G. Hautier, W. Chen, W. D. Richards, S. Dacek, S. Cholia, D. Gunter, D. Skinner, G. Ceder, and K. A. Persson, Commentary: The Materials Project: A materials genome approach to accelerating materials innovation, APL Mater. **1**, 011002 (2013).

[48] K. Parlinski, Z. Li, and Y. Kawazoe, First-principles determination of the soft mode in cubic ZrO_2, Phys. Rev. Lett. **78**, 4063 (1997).

[49] A. Togo, F. Oba, and I. Tanaka, First-principles calculations of the ferroelastic transition between rutile-type and $CaCl_2$-type SiO_2 at high pressures, Phys. Rev. B **78**, 134106 (2008).

[50] A. A. Mostofi, J. R. Yates, Y.-S. Lee, I. Souza, D. Vanderbilt, and N. Marzari, WANNIER90: A tool for obtaining maximally-localised Wannier functions, Comput. Phys. Commun. **178**, 685 (2008).

[51] Q. Wu, S. Zhang, H.-F. Song, M. Troyer, and A. A. Soluyanov, WANNIERTOOLS: An open-source software package for novel

topological materials, Comput. Phys. Commun. **224**, 405 (2018).

[52] V. Wang, N. Xu, J.-C. Liu, G. Tang, and W.-T. Geng, VASPKIT: A user-friendly interface facilitating high-throughput computing and analysis using VASP code, Comput. Phys. Commun. **267**, 108033 (2021).

[53] U. Herath, P. Tavadze, X. He, E. Bousquet, S. Singh, F. Muñoz, and A. H. Romero, PYPROCAR: A PYTHON library for electronic structure pre/post-processing, Comput. Phys. Commun. **251**, 107080 (2020).

[54] P. Giannozzi, S. Baroni, N. Bonini, M. Calandra, R. Car, C. Cavazzoni, D. Ceresoli, G. L. Chiarotti, M. Cococcioni, and I. Dabo, QUANTUM ESPRESSO: A modular and open-source software project for quantum simulations of materials, J. Phys.: Condens. Matter. **21**, 395502 (2009).

[55] P. Giannozzi, O. Andreussi, T. Brumme, O. Bunau, M. B. Nardelli, M. Calandra, R. Car, C. Cavazzoni, D. Ceresoli, and M. Cococcioni, Advanced capabilities for materials modelling with QUANTUM ESPRESSO, J. Phys.: Condens. Matter. **29**, 465901 (2017).

[56] P. B. Allen and R. C. Dynes, Transition temperature of strong-coupled superconductors reanalyzed, Phys. Rev. B **12**, 905 (1975).

[57] A. G. Kvashnin, D. V. Semenok, I. A. Kruglov, I. A. Wrona, and A. R. Oganov, High-temperature superconductivity in a Th-H system under pressure conditions, ACS Appl. Mater. Interfaces **10**, 43809 (2018).

[58] M. Schlipf and F. Gygi, Optimization algorithm for the generation of ONCV pseudopotentials, Comput. Phys. Commun. **196**, 36 (2015).

[59] Y. Zhou, W. Wei, B. Zhang, Y. Yuan, C. Chen, X. Chen, C. An, Y. Zhou, H. Wu, S. Wang, M. Qi, R. Zhang, C. Park, M. Tian, and Z. Yang, Effect of pressure on structural and electronic properties of the noncentrosymmetric superconductor Rh_2Mo_3N, Phys. Rev. B **100**, 174516 (2019).

[60] M. Zhou, Y. Gu, B. Ruan, Q. Dong, Q. Yang, G. Chen, and Z. Ren, Synthesis, structural and physical properties of new ternary metal-rich phosphides M_3Ge_2P (M = Mo and W), J. Solid. State. Chem. **316**, 123554 (2022).

[61] C. J. Bartel, A. Trewartha, Q. Wang, A. Dunn, A. Jain, and G. Ceder, A critical examination of compound stability predictions from machine-learned formation energies, npj Comput. Mater. **6**, 97 (2020).

[62] M. Aykol, S. S. Dwaraknath, W. Sun, and K. A. Persson, Thermodynamic limit for synthesis of metastable inorganic materials, Sci. Adv. **4**, eaaq0148 (2018).

[63] M. Liu, A. Jain, Z. Rong, X. Qu, P. Canepa, R. Malik, G. Ceder, and K. A. Persson, Evaluation of sulfur spinel compounds for multivalent battery cathode applications, Energy Environ. Sci. **9**, 3201 (2016).

[64] W. Sun, S. T. Dacek, S. P. Ong, G. Hautier, A. Jain, W. D. Richards, A. C. Gamst, K. A. Persson, and G. Ceder, The thermodynamic scale of inorganic crystalline metastability, Sci. Adv. **2**, e1600225 (2016).

[65] S. P. Ong, L. Wang, B. Kang, and G. Ceder, Li–Fe–P–O_2 phase diagram from first principles calculations, Chem. Mater. **20**, 1798 (2008).

[66] S. P. Ong, W. D. Richards, A. Jain, G. Hautier, M. Kocher, S. Cholia, D. Gunter, V. L. Chevrier, K. A. Persson, and G. Ceder, Python Materials Genomics (PYMATGEN): A robust, open-source PYTHON library for materials analysis, Comput. Mater. Sci. **68**, 314 (2013).

[67] See Supplemental Material at http://link.aps.org/supplemental/10.1103/PhysRevB.109.035144 for additional details about the phonon calculations, atomic sites, bands, and superconducting parameters of the corresponding Mo_3Al_2C-like phases.

[68] F. Mouhat and F.-X. Coudert, Necessary and sufficient elastic stability conditions in various crystal systems, Phys. Rev. B **90**, 224104 (2014).

[69] X.-Q. Chen, H. Niu, D. Li, and Y. Li, Modeling hardness of polycrystalline materials and bulk metallic glasses, Intermetallics **19**, 1275 (2011).

[70] W. Xie, P. Zhang, B. Shen, W. Jiang, G. Pang, T. Shang, C. Cao, M. Smidman, and H. Yuan, CaPtAs: A new noncentrosymmetric superconductor, Sci. China: Phys., Mech. Astron. **63**, 237412 (2020).

[71] G. Kuderowicz, P. Wójcik, and B. Wiendlocha, Electronic structure, electron-phonon coupling, and superconductivity in noncentrosymmetric $ThCoC_2$ from *ab initio* calculations, Phys. Rev. B **104**, 094502 (2021).

[72] L. Jiao, J. L. Zhang, Y. Chen, Z. F. Weng, Y. M. Shao, J. Y. Feng, X. Lu, B. Joshi, A. Thamizhavel, S. Ramakrishnan, and H. Q. Yuan, Anisotropic superconductivity in noncentrosymmetric BiPd, Phys. Rev. B **89**, 060507(R) (2014).

[73] D. C. Peets, A. Maldonado, M. Enayat, Z. Sun, P. Wahl, and A. P. Schnyder, Upper critical field of the noncentrosymmetric superconductor BiPd, Phys. Rev. B **93**, 174504 (2016).

[74] M. H. Fischer, M. Sigrist, D. F. Agterberg, and Y. Yanase, Superconductivity and local inversion-symmetry breaking, Annu. Rev. Condens. Matter Phys. **14**, 153 (2023).

[75] X. Zhang, K.-H. Jin, J. Mao, M. Zhao, Z. Liu, and F. Liu, Prediction of intrinsic topological superconductivity in Mn-doped GeTe monolayer from first-principles, npj Comput. Mater. **7**, 44 (2021).

[76] Z. P. Sun, C. Q. Hua, X. L. Liu, Z. T. Liu, M. Ye, S. Qiao, Z. H. Liu, J. S. Liu, Y. F. Guo, Y. H. Lu, and D. W. Shen, Direct observation of sixfold exotic fermions in the pyrite-structured topological semimetal $PdSb_2$, Phys. Rev. B **101**, 155114 (2020).

[77] X. Yáng, T. A. Cochran, R. Chapai, D. Tristant, J.-X. Yin, I. Belopolski, Z. Chéng, D. Multer, S. S. Zhang, N. Shumiya, M. Litskevich, Y. Jiang, G. Chang, Q. Zhang, I. Vekhter, W. A. Shelton, R. Jin, S.-Y. Xu, and M. Z. Hasan, Observation of sixfold degenerate fermions in $PdSb_2$, Phys. Rev. B **101**, 201105(R) (2020).

[78] G. Chang, B. J. Wieder, F. Schindler, D. S. Sanchez, I. Belopolski, S. M. Huang, B. Singh, D. Wu, T. R. Chang, T. Neupert, S. Y. Xu, H. Lin, and M. Z. Hasan, Topological quantum properties of chiral crystals, Nat. Mater. **17**, 978 (2018).

[79] Z. S. Gao, X.-J. Gao, W.-Y. He, X. Y. Xu, T. K. Ng, and K. T. Law, Topological superconductivity in multifold fermion metals, Quantum Front. **1**, 3 (2022).

[80] S. Zeng, Y. Zhao, G. Li, R. Wang, X. Wang, and J. Ni, Atom table convolutional neural networks for an accurate prediction of compounds properties, npj Comput. Mater. **5**, 84 (2019).